Designing, Modeling, and Casting of a circa 1830 Inspired Bowie Knife

Manuscript prepared by Manuel Umanzor

Team Members: Manuel Umanzor, Tristan Pagkalinawan, Bryan Staha, Cole Manfred, Michael Coyle

Faculty Advisor: Dr. Alan P. Druschitz

Virginia Tech, Department of Materials Science and Engineering

Partner Foundry: **Midwest Metal Products, Winona, MN**

Introduction

The history of the Bowie knife is intertwined with legends, and its origin has been proven difficult to trace. Regardless of the many exiting accounts, it seems certain that its design may be attributed to the Bowie family, rather than an individual member. Nonetheless, the facts are somewhat diluted with myths, and the many accounts of the creation of such iconic weapon. Some of these versions point towards Rezin Bowie, father of James Bowie, as the designer. According to this account, this blade was designed as a hunting knife, and Rezin Bowie once injured himself when lost grip of his knife, after that he asked a blacksmith by the name Jesse Cliffe to add a guard. In a similar tale, James Bowie's brother, Rezin P. Bowie took a high quality (as per the era's standards) steel file to the aforementioned smith, Cliffe, and tasked him with the design and manufacture of a blade that would no slip his hand, this blade, apparently was later on given to James Bowie in preparation for the famous "Sandbar Duel". Yet another version, commonly found in literature involves James Bowie himself, the latter, while engaged in battle against Mexicans, broke off his sword to, approximately, fifteen inches from the hilt [1].

In a sense, and in the words of Dobie [2], the bowie knife and its history are objects of legend such as king Arthur's "Excalibur", or Sigmund's "Gram". It is possible that due to popularity increase of the original design (whichever it might be), some people sought out to make profit of the myth behind this legendary blade. According to the facts found by Norman Flayderman during his research, at some point in history a British manufacturer called Sheffield Cutlers flooded the American market for nearly a century with Bowie knives, preying on values such as patriotism [3, 4].

The facts behind the origin of this American icon might be lost, however, the outstating characteristics and popularity of this knife are undeniable. Even to this date, the Bowie knife has a number of uses, such as hunting, chopping, and even hammering.

Design

The works of Scott [1], indicate that the original blade was tempered almost to perfection, it was about ten to fifteen inches in length, approximately two inches on the widest section, and had the well-known concave (or clipped) tip. Most importantly, is the lack of straight lines that inspired the hereafter proposed design.

Figure 1 exhibits a circa 1830 Bowie knife, which as per several online sources belonged to Jesse Robinson [5, 6]. This specimen provided most of the inspiration for the design presented within this report. After some modifications, the final model is depicted by Figure 2; the brass back was replaced with a fuller to

reduce weight, and due to manufacturing process employed, the brass ferrule and the leather washer were omitted. Moreover, as per competition design constraints, the knife includes a cast in guard and pommel, the latter is not shown in CAD model. A major modification from the 1830s design lies in the tang, instead of following the "hidden" design, a "true" option was chosen. Key reasoning behind this adjustment is derived from the centerline shrinkage inherent of the casting process [7], therefore, this portion of the knife was made wider in order to improve strength.

As mentioned above, the blade of this knife does not have straight lines, hence, a multi-point spline was employed to model the cutting edge, and large radii were used to define its back and convex tip.

Figure 1. Circa 1830 Bowie knife, from the Joseph Musso collection. Image obtained from [6].

Although not shown in Figure 2, the final model for casting does not have a sharp edge, however, bevels were considered for two main reasons; one to promote directional solidification, and to provide a guide for grinding after casting. General consensus regarding thickness lies between $3/16$ and $1/4$ in, moreover, final dimensions, also account for approximately 3% volumetric shrinkage which is common for cast steels [7].

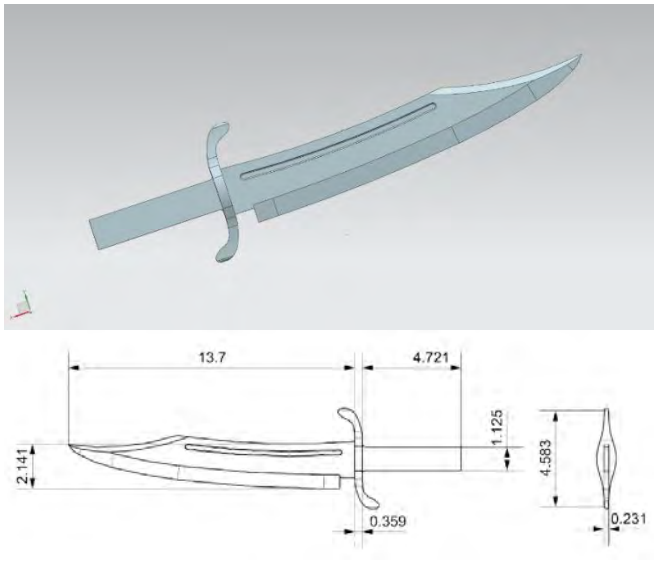

Figure 2. Virginia Tech model by Team A. Normal view (Top), and dimensions (bottom).
Not to scale, dimensions in inches

Cast Alloy – H13 Steel

In spite of the fact that H13 Steel is not a common option for knives, it was the steel recommended by our foundry partner for this project. H13 steel ha excellent resistance to thermal shock, good fracture toughness, and considering the manufacturing process, it becomes an interesting candidate for the rather long knife mentioned earlier [8]. In general, this alloy belongs to a category known as chromium hot-work steels, and they can be thru hardened in sections up to six inches, additionally, they have good resistance to heat softening because of the addition of carbide-forming elements such as chromium, and vanadium [9]. Typical room-temperature mechanical properties are summarized in Table 1.

Table 1. Typical room-temperature mechanical properties of H-13 steel bar oil quenched from 1010 °C and tempered at different temperatures [9]

Tempering Temperature[1]	Tensile strength	Yield strength	Elongation In 4 D	Reduction in Area	Charpy V-notch impact energy		Hardness
(°C)	(MPa)	(MPa)	(%)	(%)	(ft-lb)	(J)	(HRC)
527	1958	1572	13.0	46.2	12	16	52
554	1843	1530	13.1	50.1	18	24	50
574	1730	1469	13.5	52.4	20	27	48
593	1578	1365	14.4	53.7	21	28.5	46
604	1496	1296	15.4	54.0	22	30	44

[1]Double tempered, 2 + 2 hours

The H-13 steel was prepared using a 300 lb capacity induction tilt furnace. First, 1045 and 1008/1010 plain carbon steel were placed inside the crucible. After the plain carbon steel melted, the silicon and manganese quickly formed a liquid slag, which was removed from the melt. Once the latter was removed, the carbon in solution started to react with oxygen in solution and the process knows as carbon boil began. This process was allowed to continue and reduce the carbon content of the base charge. When the carbon boil began to subside, pure aluminum shot was added to kill the steel and stop the carbon boil. Based on prior experience, chemical composition of the base charge would be approximately 0.007 wt% Si, 0.13 wt% Mn, and 0.15 wt% C. Next, the alloying elements that do not readily oxidize (Cr, Mo, V) were added. After the alloying elements had sufficient time to go into solution, the carbon (in the form of Sorelmetal®) was added. Sorelmetal® was used instead of carbon riser to maximize recovery and minimize sulfur pick-up. After the Sorelmetal® had sufficient time to melt and the carbon to go into solution, the heat was brought to the desired pouring temperature. At this time, 75% FeSi and 70% FeMn were added. Shortly after adding the Si and Mn, a chemistry sample was taken, the temperature of the molten metal was determined, the furnace was tapped, and the castings poured. The base steel charge and the carbon boil are shown in Figure 3.

Figure 3. Melting process; left: base steel charge, right: carbon boil (rectangle shows the Sorelmetal®)

Chemical composition (Table 2) was determined using a Bruker Q4 Tasman Advanced CCD-Based optical emission spectrometer. Two heats were melted and cast. The chemistry sample was taken from the furnace a few minutes before pouring. The first heat was slightly low in C, Mo, and V but slightly high in Mn. Since C is a critical element for achieving hardness in a knife, adjustments were made to the second heat. The carbon content of the second heat was much more desirable plus the Cr and Mo contents were increased. The Si and V were just slightly low and the Mn was now in spec. We do not know how accurate the measured P content was (these readings seem high) and our spectrometer did not provide an accurate S content for the standardization method used.

Table 2. Measured chemical composition of our castings and the standard specification (wt %).

Element	C	Si	Mn	Cr	Mo	Ni	V	P	S
1st Heat	0.31	0.83	0.77	4.93	1.03	0.07	0.78	0.065	<0.150
2nd Heat	0.44	0.66	0.43	5.33	1.28	0.08	0.73	0.085	<0.150
Specification [9]	0.32-0.45	0.80-1.20	0.20-0.50	4.75-5.50	1.10-1.75	0.30 Max	0.80-1.20	0.030 Max	0.030 Max

Mold Design and Manufacturing

The model depicted by Figure 4 was set for a vertical pour, hence, a single gate, a filter print, and a pour cup were added. Final mold was then created in CAD by means of a Boolean subtraction, and it consists of two parts that were sectioned by using the centerline of the knife as a guide (See Figure 4).

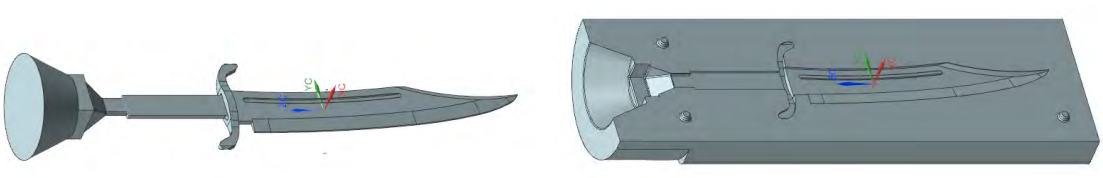

Gated

Left-hand side

Figure 4 CAD modeling of the mold

Molds were additively manufactured (AM) via the binder jetting process, in which a binding agent, usually in liquid form, is selectively deposited onto a build chamber filled with powder particles, in this case fine silica sand. This deposition process is carried out in stages or layers, after one layer is deposited, a roller spreads a new layer of media while the build platform is lowered simultaneously, this sequence is carried on until the mold is complete. Figure 5 shows a schematic breakdown of the process.

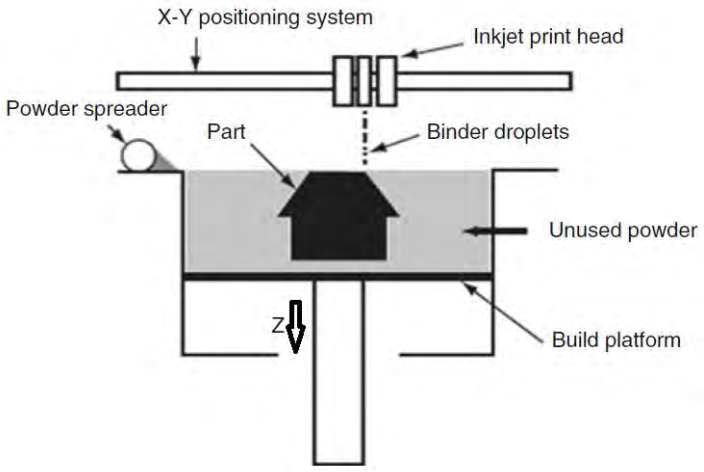

Figure 5. Schematic description of the binder jetting process [10]

Last stage of the binder jetting process consists on allowing for the binding agent to cure, such that the molds are hard enough to be moved. These molds were cleaned with dry compressed air afterwards (Figure 6)

Figure 6. Additively manufactured two-piece sand mold courtesy of ExOne

Modeling the Casting Process

Before proceeding with casting of the knife, the mold filling and solidification processes were modeled using MAGMASOFT® [11]. This tool helped validate the mold design, and predict potential issues (e.g. hot tears, centerline shrinkage, and porosity) with the casting before even melting a single ounce of metal. From the MAGMASOFT® database, material X40CrMoV5_1 was selected to model the H-13 steel, remaining input parameters are summarized in Table 3.

Table 3. General parameter selection for Magma® model

	Filename	Description
Metal	X40CrMoV5_1	Hot working steel with 0.4% C, 5% Cr and 1% Mo, and less than 1% V
T_0 (°C)	1600	Initial Temperature
Mold	Furan	Furan bonded silica sand
Filter	CeramicFoam_40ppi	

After the first iteration, a large cavity was noted at the section where the tang connects to the integrated guard (Figure 7). During solidification, the thick portion of the guard constitutes a local hotspot that would be cut off from feeding.

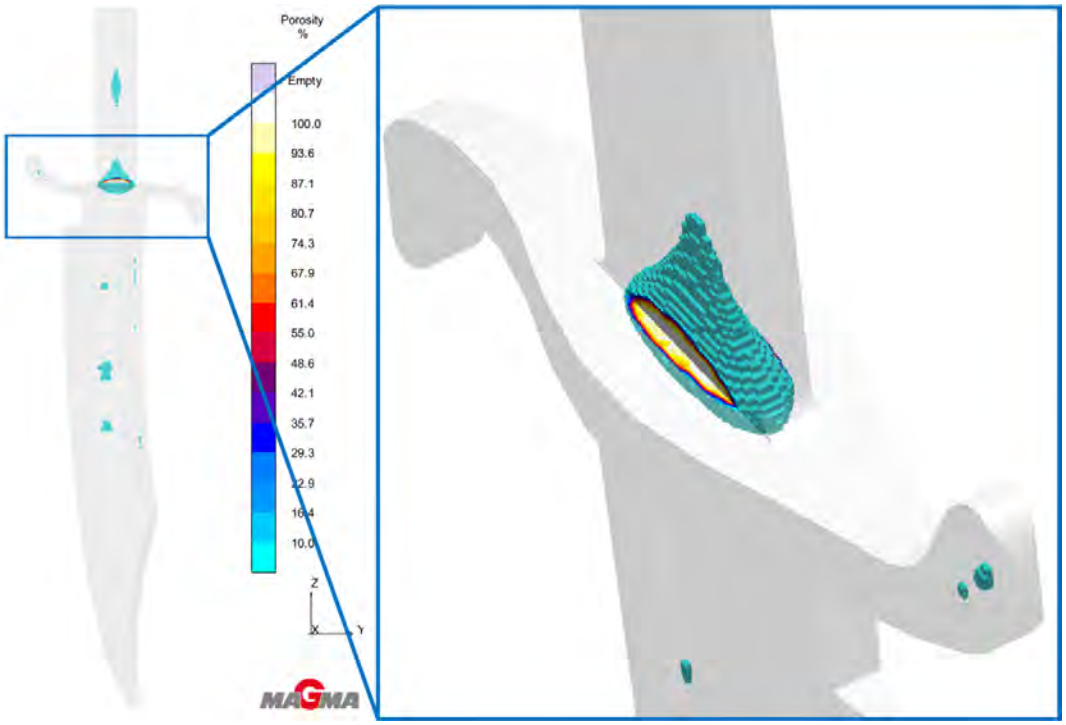

Figure 7. Porosity result, X-Ray feature on. Zoomed in portion shows a large open cavity

Another way of visualizing this outcome, entails on using the "fraction liquid" result, and since feeding effectivity was defined at 30%, in other words, as soon as the molten metal reached this percent-solid value, it was not able to flow anymore (see Figure 8). On a positive note, the analysis confirmed that having bevels at the cutting edge was beneficial to promote directional solidification, which as stated earlier was part of the design intent.

Figure 8. Fraction liquid fringe plots at different times. X-ray scale set such that any volume with less than 70% liquid is hidden from view.

In light of the restrictions posed by the COVID-19 crisis, it was decided to modify the existing molds, rather than ordering a new set, therefore the CAD model was modified as follows: the tang section was increased, approximately three times, and the gate was designed twice as large, in both cases, the increase was considered along the thickness (x-axis as per models previously shown). Figure 9 provides a graphical representation of the modifications, as well as a comparison with the initial design.

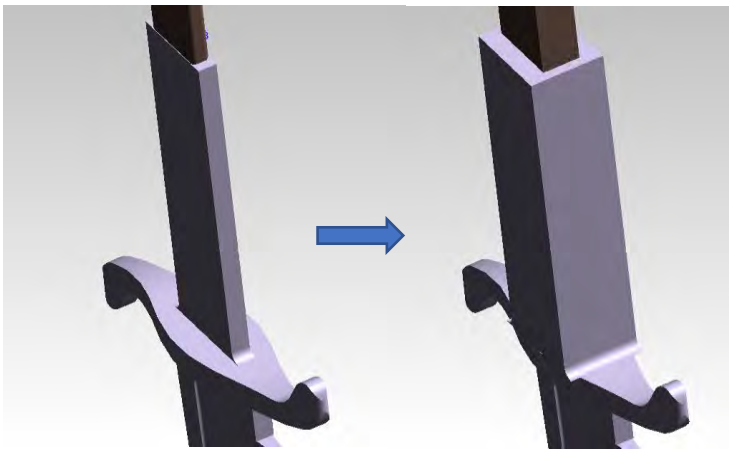

Figure 9. CAD images showing the modifications made to the tang and gate.

Upon examination of the porosity results, albeit not optimum, the outcome was satisfactory; not only the open cavity at the guard-tang connection was accounted for, and the centerline shrinkage was displaced towards the gate connection (Figure 10). The solidification sequence shown in Figure 11 indicates that the volume of metal around the guard area was no longer interrupted from feeding.

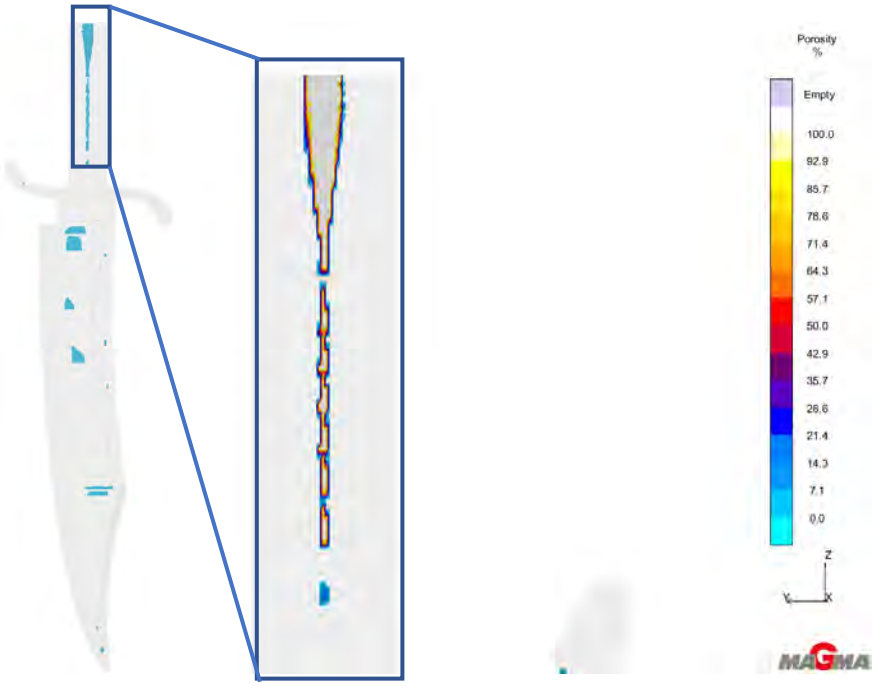

Figure 10. Porosity result of the modified design, the callout shows a clipped view of the centerline shrinkage.

Figure 11. Solidification sequence as seen from the fraction liquid result

Upon examination of the solidification results, specifically the temperature at the end of solidification, elevated values were observed at critical areas with straight angles (Figure 12). This, in turn provided information regarding additional modifications needed to be done to the AM molds.

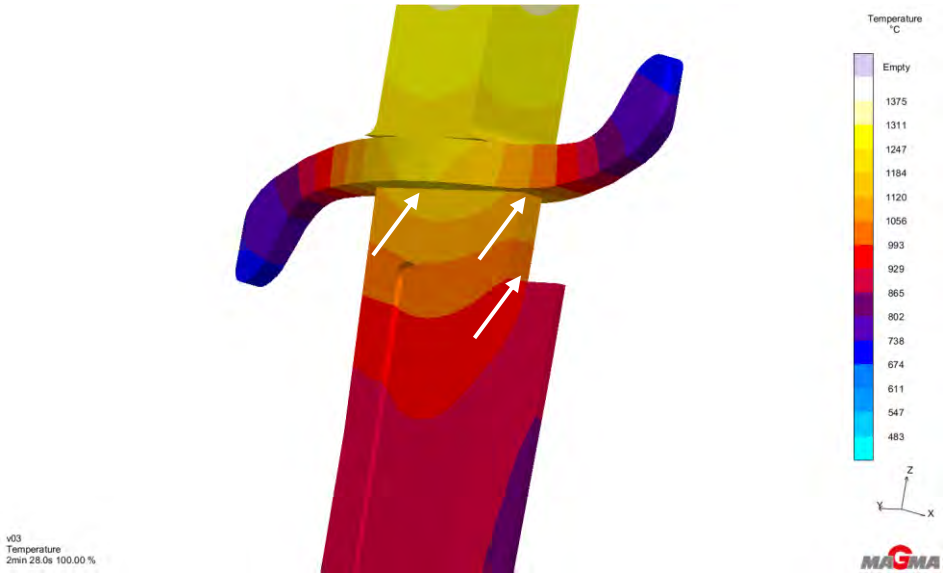

Figure 12. Temperature contour plot at the end of solidification; white arrows indicate areas of possible concern.

Manufacturing the Knives

With the information provided by the MAGMASOFT® results, the molds were modified in order to help mitigate casting defects. This labor was performed by hand, and even though measurements were taken with a depth gauge, some small inconsistencies were expected (Figure 13).

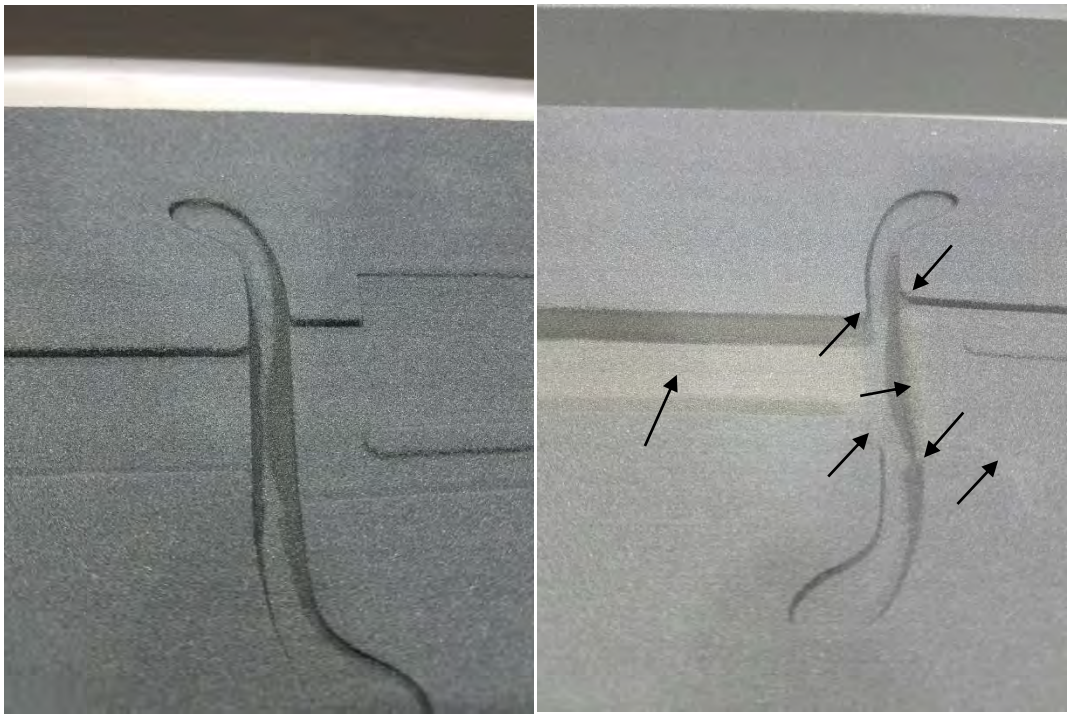

Figure 13. Close up view of critical areas of the molds. Left: initial state, and Right: Arrows point at the modifications

Once the alloy was ready and at initial temperature, the molds were poured by hand. The process was carried on sequentially, in other words, the furnace was not tilted back to its resting position, it was deemed that the temperature was sufficiently high in order to pour all molds without the need to re-heat the molten metal (Figure 14). A total of five molds were poured from two separate heats, which were made on two different dates.

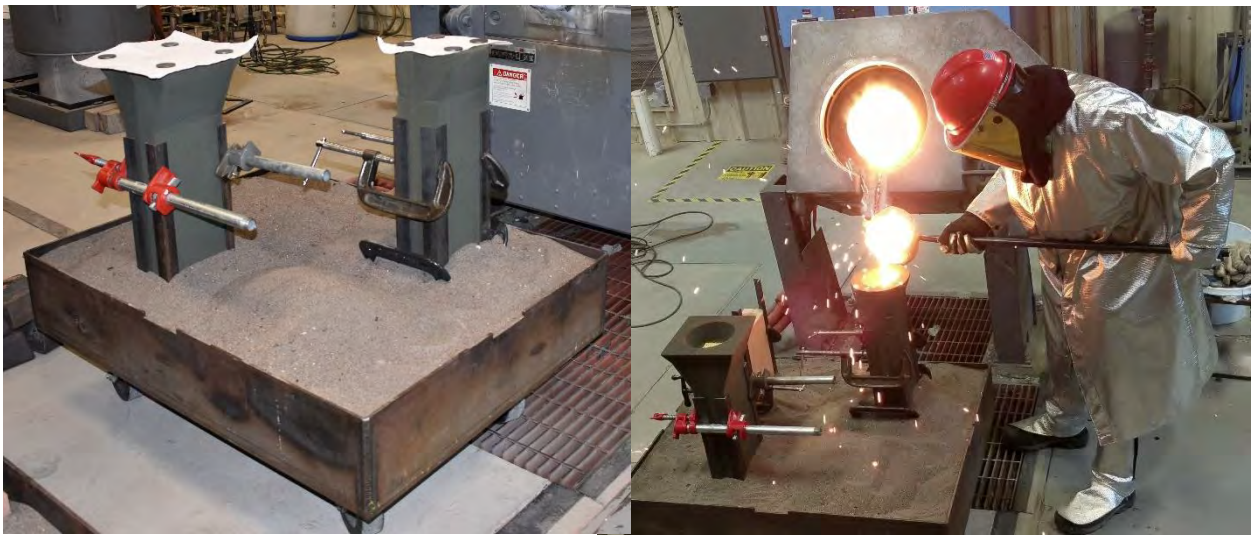

Figure 14. Pouring Bowie knives in H-13 steel. The mold on the far left-hand side of the cart had a filter.

During pouring, it was noted that the flow of molten metal on the mold with filter was rapidly interrupted, this was perhaps linked to the filter itself. Castings were allowed to solidify and cool down before shake out. All contrasting cases are shown by Figure 15, with the following outcomes; mold without filter was filled completely, incomplete fill for the mold with filter, and the last pour ended up in incomplete fill due to low temperature.

Figure 15. As-cast knives showing different outcomes: a) complete fill without filter, b) incomplete fill with filter, and c) incomplete fill due to low pouring temperature.

Components of the gating system were cut from the casting with an abrasive wheel, it was anticipated that due to carbide formation, regular cutting tools were not suited for this task. At this point, gaiting system design proved convenient, provided that a single cut was needed in order to remove the excess metal. Soon after, it was noted that the MAGMASOFT® prediction for porosity turned out to be comparable (Figure 16). Next stage consisted on cleaning the castings, first using a grinding belt, and later grit blasted, and at this point hot tears were noted on some specimens (Figure 17). A summary of outcomes is provided in Table 4.

Figure 16. Cross-sectional view showing centerline porosity

Table 4. Summary of outcomes

Knife	Heat	Pouring Temperature (°C)		Filter	Hot Tearing	Fill
1	1	Initial	1634	No	No	Complete
2		Final	1619	Yes	No	Incomplete
3	2	Initial	1646	No	Yes	Complete
4				No	No	Complete
5		Final	1477	No	Yes	Incomplete

Figure 17. Hot tears developed in some of the castings. Neither of these castings appeared to have fillets around the sharp corners.

The as-cast knives were very difficult to grind due to the high as-cast hardness. Since the thickened tang required significant grinding, the castings were annealed according to the process outlined in Table 5. The annealing process reduced the hardness to <20 HRC (9 HRC measured). The tang was then ground to approximately 3/8 in (10 mm), and the centerline porosity was used as a guide to drill and tap a hole, which later served as the anchoring point for the pommel. As shown in Figure 18, holes for the handle and for the pommel were drilled before the final hardening heat treatment. To compensate for a small amount of potential de-carburization during hardening and tempering, the cutting edge was not ground at this time.

Table 5. Annealing Process Parameters
(annealing performed by Southwest Specialty Heat Treat, Wytheville, VA)

Stage	Temperature (°C)	Dwell Time (hr)
Heat up[1]	871	2
Cool down	760	6
Cool down	25	Overnight

Figure 18. Knife ready for hardening and tempering.

Continuing with the manufacturing process, for the knife to have appropriate mechanical properties it was hardened and tempered (Table 6). The final hardness of the knife was 50-52 HRC, as expected. The final manufacturing steps consisted on attaching the handle and pommel, as well as cleaning and sharpening the edge (Figure 19). A 25° blade angle was chosen for the cutting edge. The pommel was made from yellow brass, and the finished knife is 478 mm (18 13/16 in) long, with a 333.4 mm (13 1/8 in) blade. The blade is 52.39 mm (2 1/16 in) at its widest section, whereas its overall thickness along the spine is 5.58 mm (0.22 in). Final weight of the knife including handle scales and pommel was measured at 980.67 g (2.16 lb).

[1] Prior to loading the knives in the furnace, they we wrapped in stainless steel foil for protection.

Table 6. Hardening Heat Treatment Parameters
(hardening and tempering performed by Southwest Specialty Heat Treat, Wytheville, VA)

Process Step	Temperature (°C)	Dwell Time (min)	Remarks
Initial Heat up[2]	843		equalize, endo atm
Austenitize	1010	30-45	endo atm
Air cool	65	15-20	forced air
First temper	537	120	
Air cool	25		forced air
Second temper	537	120	
Air cool	25		forced air

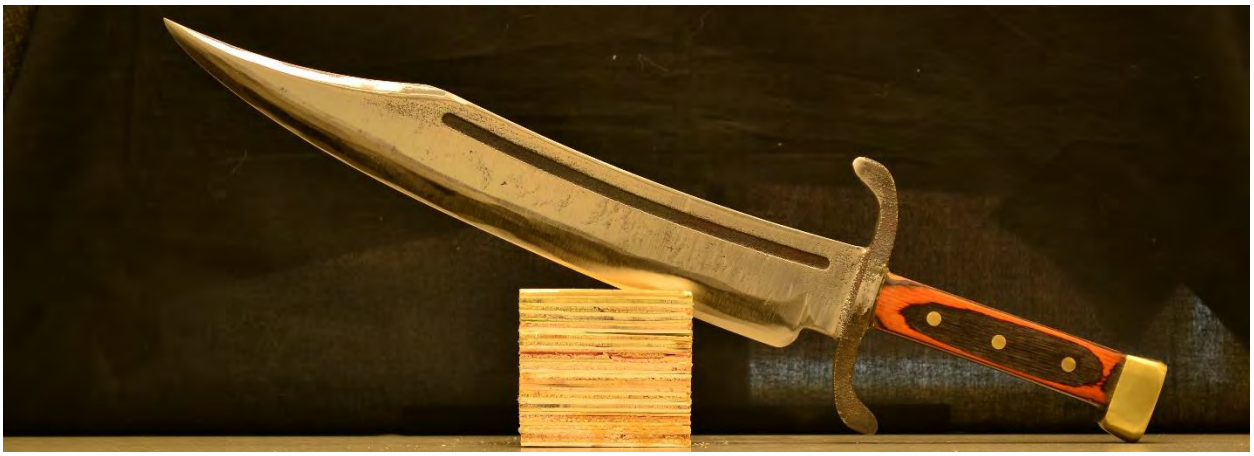

Figure 19. Finished knife, including handle and pommel

Performance Modeling

Performance of the blade was modeled using nonlinear finite element analysis (FEA), and for this purpose the software LS-DYNA® was selected due to its highly non-linear capabilities and explicit time integration [12]. Explicit time integration requires, not only discretization of the continuum in space, but in time as well, and this requires a very small time-step, which in turn could become computationally expensive in the case of fine meshes, hence, and axisymmetric model was generated with proper constraints and boundary conditions. Figure 20 exhibits the two scenarios studied as part of this project; a 9 mm FMJ round being fired directly at the blade, and a high velocity swing of the knife against a 1006 steel rod. Details of both models are provided in Table 7.

[2] Parts put in furnace with an endothermic atmosphere furnace with 4°C dew point at 843°C then equalize

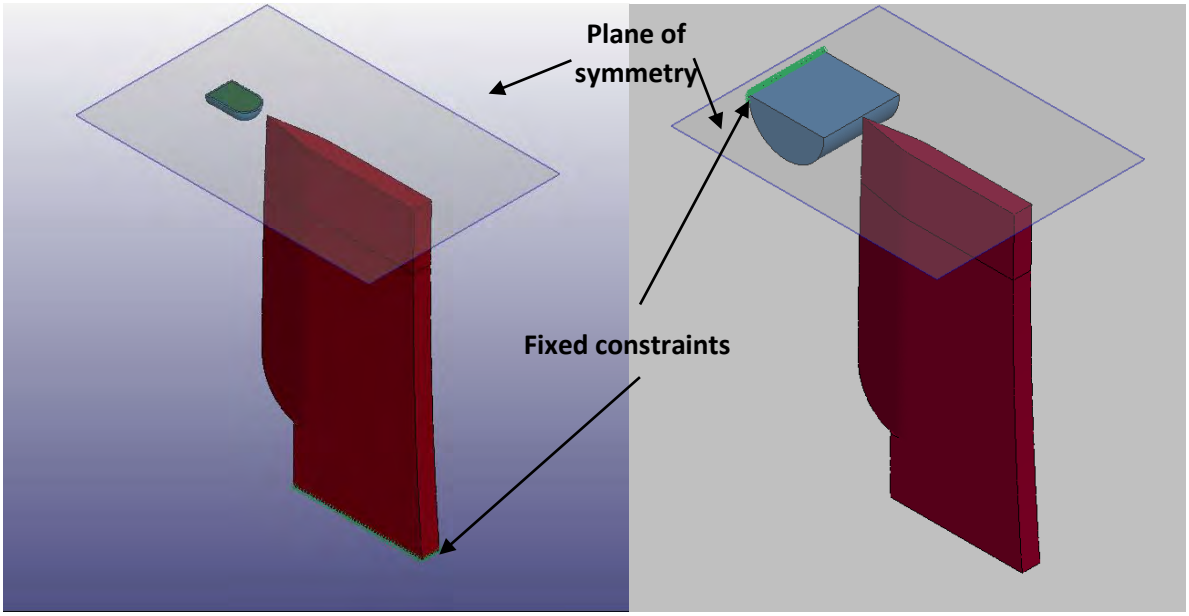

Figure 20. Axisymmetric models: 9 mm FMJ round impact on knife (left) and knife strike on 1006 steel rod (right)

Table 7. Materials, and material models employed for FEA modeling

9 mm round model

Component	Material	Material model	v_0 (m/s)
Knife	H-13 Steel (~52 HRC) [13]	Simplified Johnson-Cook	Stationary
Projectile Jacket	Copper (Cold rolled) [14]	Simplified Johnson-Cook	250 [15]
Projectile Core	Lead [15]	Bi-linear	

1006 steel rod model

Component	Material	Material model	v_0 (m/s)
Knife	H-13 Steel (~52 HRC)	Simplified Johnson-Cook	27.7 [16]
Rod	1006 Steel [17]	Simplified Johnson-Cook	Stationary

With the intention of further simplifying the model, instead of generating one angle for the cutting edge and another one for the bevel, a single gradient of 20 degrees was created, therefore, the number of sharp edges around the first impact zone is just one. Erosion strain was set as the failure criteria for both scenarios, and under this mathematical framework any given element is deleted from the calculation once

its effective plastic strain reaches the value set for erosion, this criterion was set as the true plastic strain at fracture.

Figure 21 displays a sequence of images regarding the 9 mm round FMJ ballistic model. At a first glance, it was noticed that the knife splits the projectile in half, while taking significant damage in the process (approximately 4 mm around the impact zone).

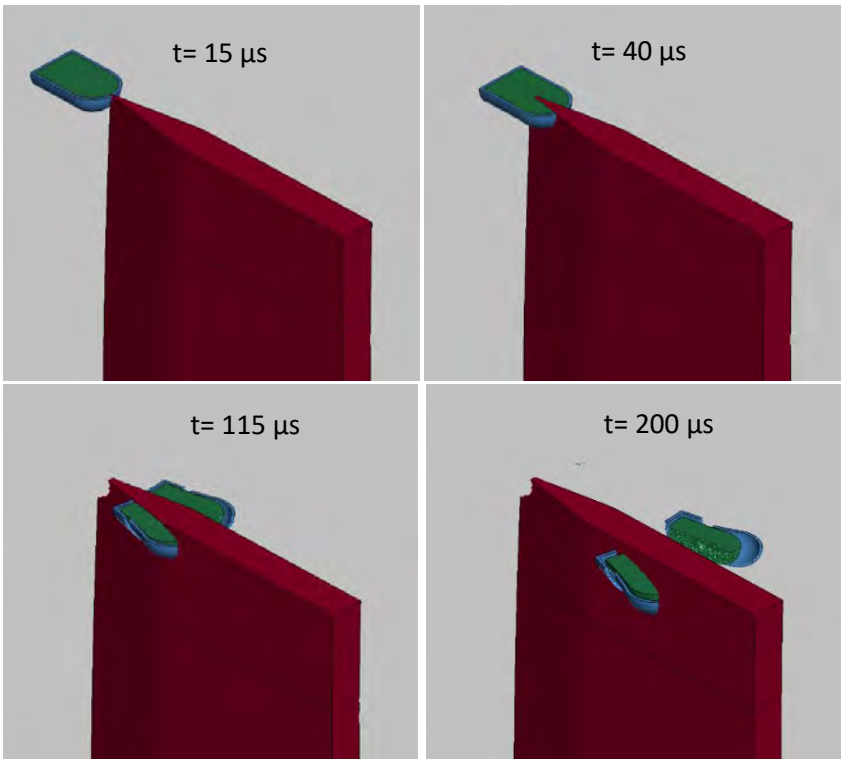

Figure 21. Impact sequence of 9 mm round on knife. The projectile was split in half; however, the edge took damage.

Damage taken by the edge was enhanced due to the intrinsic nature of the mathematical model employed; one could think in terms of the most fundamental definition of stress, $\sigma = F/A$, and since the area at the very tip of the edge is nearly zero, the stress level would be infinitely high. A probe was used to measure the effective stress taken by the first element of the knife to come in contact with the projectile, and the value was 2220 MPa, which is much higher than the typical stress at fracture [14] of H-13 steel, and its associated plastic strain is larger than the failure criteria, hence, that element was soon eliminated from the calculation. At the end of the simulation time, the residual velocity of the projectile was 149 m/s, as calculated from the lead core.

The second scenario resulted on a similar outcome from the perspective of the knife (Figure 22), which took significant damage. In this case, however, deformation of the target was a 1 mm deep indentation. The blade reached a complete stop, before bouncing back off the target (Figure 23). Provided that the geometry of the blade was the same for this setting, the above-mentioned mathematical explanation held

true. Similarly, stress level measured at the first element of the blade to come in contact with the mild steel rod was measured at 2240 MPa.

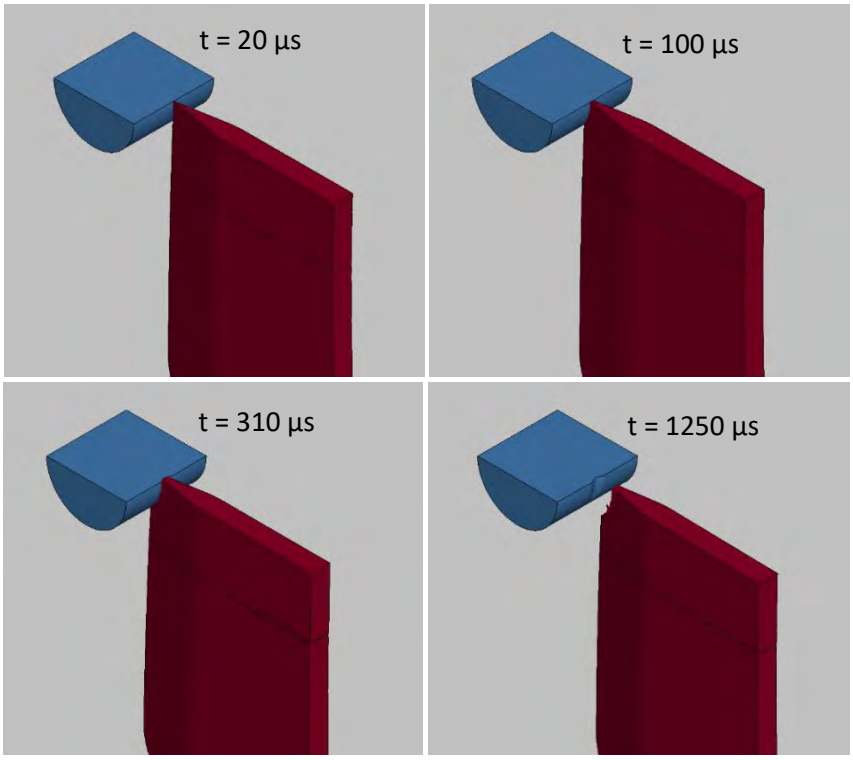

Figure 22. Sequence of knife impact on mild steel rod. At the end of the simulation time, a clear indentation was noted on the steel target.

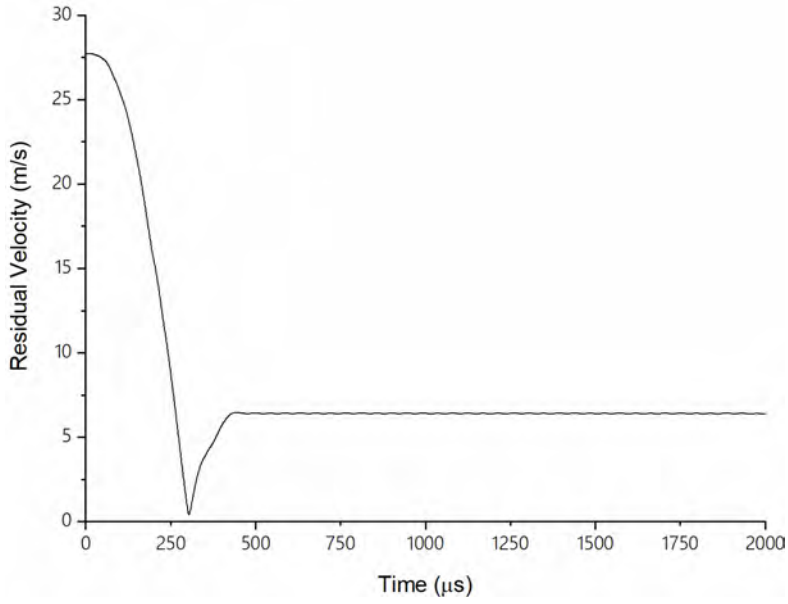

Figure 23. Knife velocity history, the graph shows when the knife comes to a complete stop, and then bounces back from the target.

Suggestions for Future Work

Even though increasing the cross-sectional area of the tang helped addressing the otherwise potential weak spot, it also gave rise to extended finishing tasks, such as grinding the tang down to reasonable thickness. Upon examination of the thermal modulus result, it may have been possible to address this issue by adding risers to the gating system, and thus, a series of studies were performed using MAGMASOFT®. First, thermal modulus of the original design was taken into consideration for the initial design, the fringe plot indicated that its most extreme value was rounded at 0.4 cm, subsequently the hot spot result was employed to analyze how far the issue extended (Figure 24).

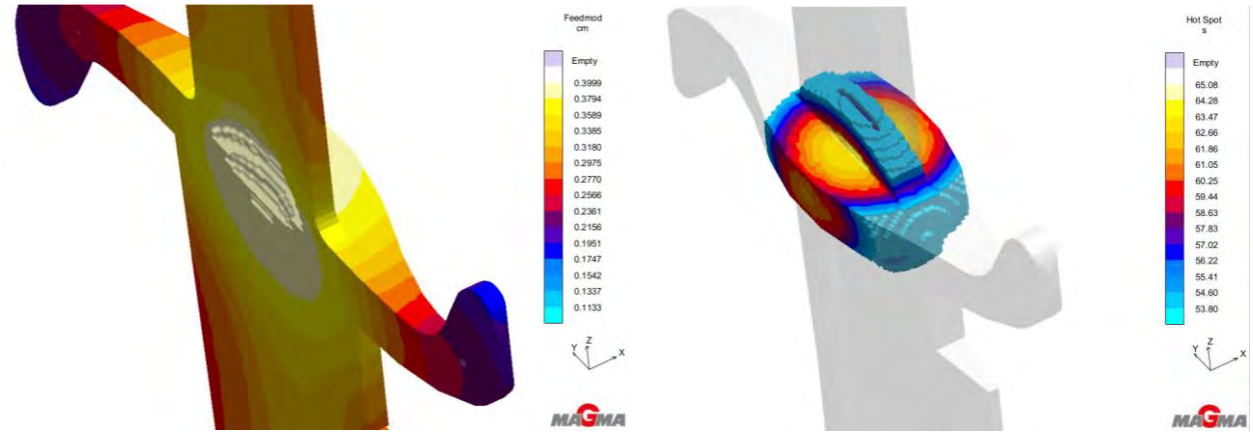

Figure 24. Thermal modulus result (left) and hot spot criteria (right)

Given the symmetric nature of the design, it was decided to add two risers on each opposing side of the hot spot. Dimensions of the risers and their respective necks were calculated under the following assumptions; using the thermal modulus of the casting as baseline, the modulus of the riser and the riser neck were increased by 20% and 10%, respectively. Initial dimensions are summarized in Table 8.

Table 8. Initial dimensions of risers and the riser contacts

Component	Parameter (mm)	
	Diameter	Height/Length
Risers	25	37.5[a]
Riser contact	9[b]	10

[a] Riser height was assumed as $1.5D_R$

[b] Constrained by the thickness of the guard

The initial model was then modified to include risers and their respective necks. Base of the risers was modeled as a hemisphere, and the rest of the volume was defined as a tapered cylinder with 2° draft. Upon visual evaluation, the relative height of the risers with respect to the tang of the knife seemed short, therefore a 25 mm parametric extension was added to each riser (Figure 25). A design of experiments

(DOE) job was created under the optimization perspective, and with the intention of constraining the model to be symmetric only six designs were considered (instead of running a full factorial), in order to execute this DOE, the height of the riser extension was varied from 0 mm to 25 mm at 5 mm increments.

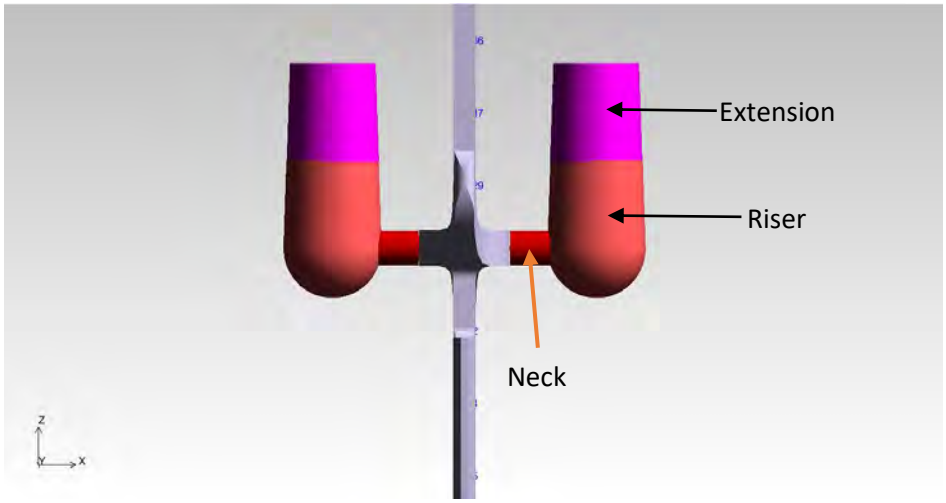

Figure 25. Final design, including the parametric risers for DOE job.

Reduce porosity was selected as the objective for this DOE, and special attention was given to the region previously shown in Figure 24. Relative values indicate that adding 20 mm more to the height of both risers would provide the better outcome in reducing porosity (See Table 9).

Table 9. Optimization results

Design	Extension (mm)		Rank	Reduce porosity	Porosity volume[ii] (mm^3)
	Riser 1	Riser 2			
0[i]	0	0	-	-	1453.40
1	5	5	5	1.57	1453.15
2	10	10	4	1.57	1453.99
3	15	15	3	1.57	1452.27
4	20	20	1	1.55	1411.77
5	25	25	2	1.55	1412.65

[i]Baseline

[ii]Measured at the section of interest

A graphical representation of the first four experiments (ordered by rank) is shown in Figure 26. In all cases, and from a qualitative standpoint, differences were noted. In order to promote piping in,

"firecrackers" were added to both risers, and their volume loss was compensated by increasing the height of the risers, such that the volume remained unchanged. Continuing with the task of minimizing the open cavity at the region where the guard connects to the tang, a parametric study was conducted to assess the effect of the riser necks. On the first iteration, it became evident that the length of the riser necks played an important role into mitigating the impact of shrinkage.

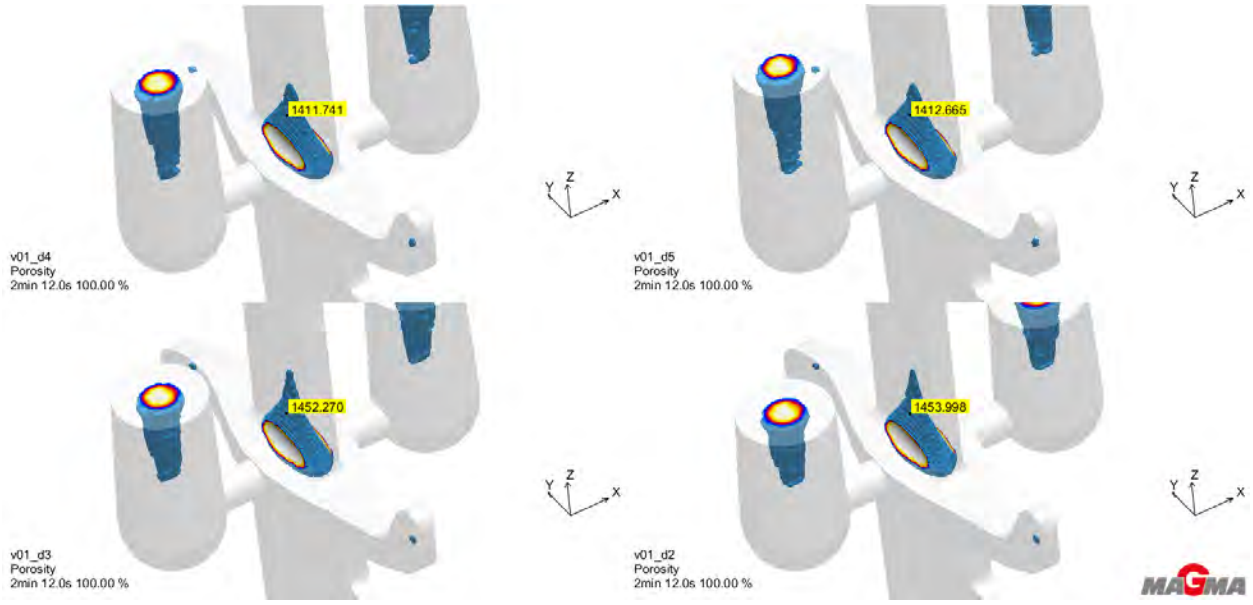

Figure 26. Porosity result of the four highest ranked designs

Reducing the neck length helped, not only in reducing the porosity volume at the spot of interest, but it also changed the time at which this volume becomes isolated (Table 10). A graphical representation of the latter is shown by Figure 27.

Table 10. Effect of riser neck length

Design	Neck length (mm)	Porosity volume (mm^3)	Time at isolation (sec)
A	10	945.40	17.12
B	5	323.63	25.76
C	2.5	99.19	30.89

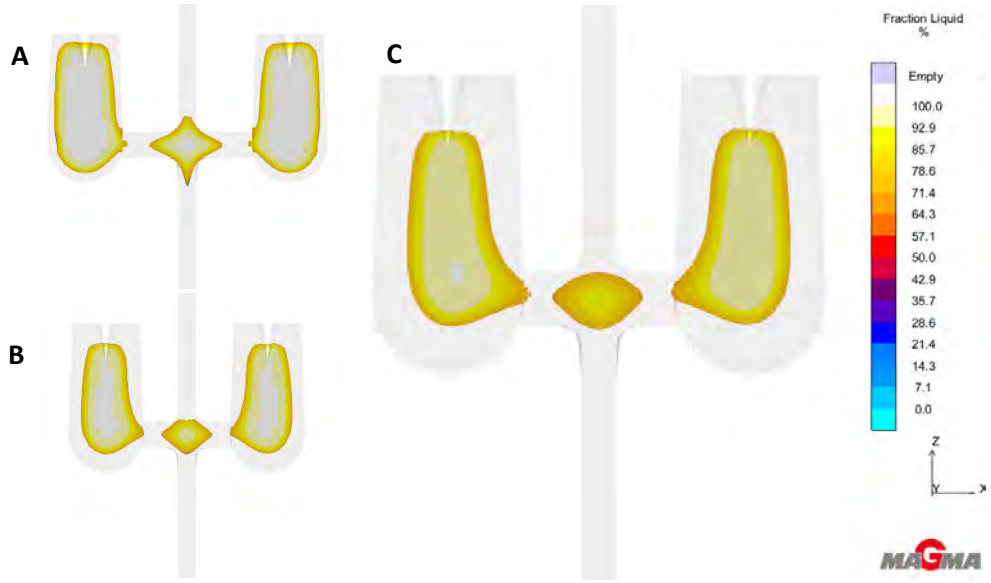

Figure 27. Liquid fraction results as function of riser neck length: A) 10 mm, B) 5 mm, and C) 2.5 mm

Another issue encountered during the solidification process was the presence of hot tears. In an attempt to lessen the formation of this type of defect, fillets were created on all critical corners (similar to Figure 13). With this in mind, a stress simulation was performed, and the casting was allowed to cool down to 100 °C, the simulation result indicated that there is still a risk for hot tearing at the sharp corners, particularly at the section of concern (Figure 28).

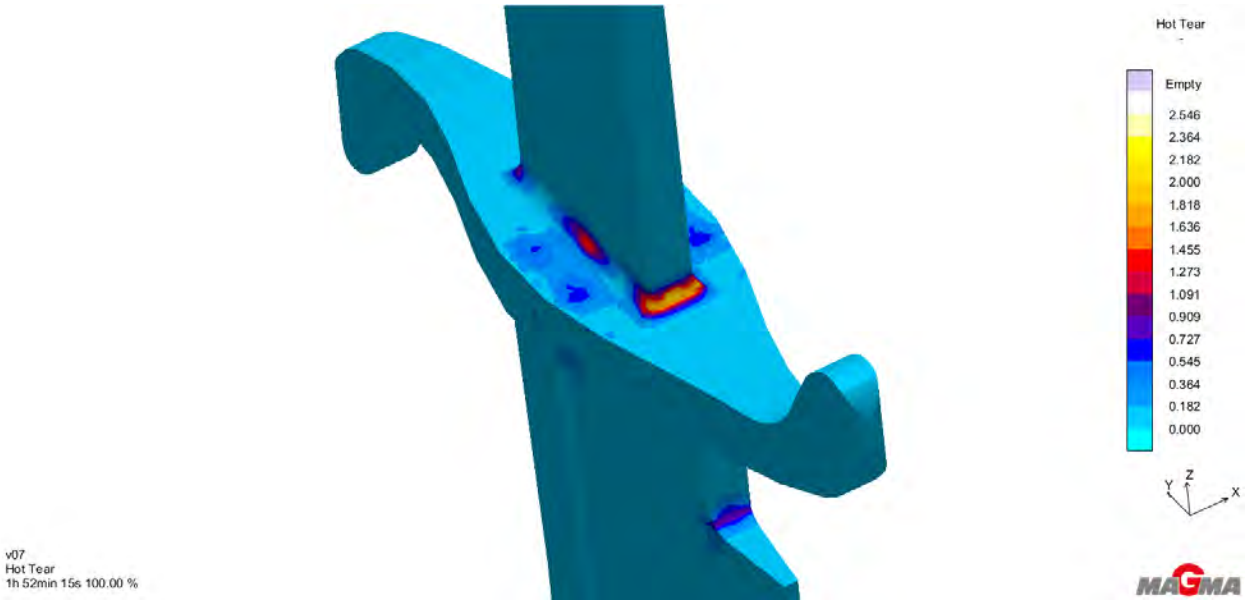

Figure 28. Areas with a high risk for hot tearing

The modifications made to the initial design have the potential of alleviating most of the defects that they were intended for, however, additional tasks might be required in order to further improve soundness of this casting, particularly, porosity in the blade itself was not addressed at the time of this report (See Figure 29).

Figure 29. Porosity results for the complete knife; note that there are numerous areas of concern on the blade but these are generally in thick areas.

Acknowledgements

The authors would like to thank Mark Adamovits from ExOne for providing the AM sand molds used for this project, Jeanne Wagner from Midwest Metal Products for donating the base steel and alloying elements necessary to prepare the H-13 alloy. Annealing and final heat treatment was performed by David Carpenter from Southwest Specialty Heat Treat Inc. Special thanks to Genevieve Gural for her support during mold setup and pouring.

References

[1] R. F. Scott, "Who Invented the Bowie Knife?," *Western Folklore,* vol. 8, no. 3, pp. 195-201, 1949, doi: 10.2307/1497920.

[2] J. F. Dobie, "BOWIE AND THE BOWIE KNIFE," *Southwest Review,* vol. 16, no. 3, pp. 351-368, 1931. [Online]. Available: www.jstor.org/stable/43461851.

[3] G. M. Bakken, "The Bowie Knife: Unsheathing an American Legend," *Montana: The Magazine of Western History,* vol. 56, no. 2, pp. 80-80, 2006. [Online]. Available: www.jstor.org/stable/4520801.

[4] N. E. Bender, "The Bowie Knife: Unsheathing an American Legend by Norm Flayderman," *The Journal of American Folklore,* vol. 120, no. 477, pp. 373-374, 2007, doi: 10.2307/20487570.

[5] M. I. Humphrey. "The Bowie Knife…Fact, Myth, Legend." https://relentlessknives.com/BowieHistory.html (accessed.

[6] P. Spangenberger. "Fighting Blades of the Frontier." https://truewestmagazine.com/bowie-knife-fighting-blades-of-the-frontier/ (accessed.

[7] F. P. Schleg, *Technology of Metalcasting*. Schaumburg, IL: American Foundry Society, 2003.
[8] W. E. Bryson, "Heat Treatment - Master Control Manual," ed: Hanser Publishers, pp. 224-226.
[9] A. M. Bayer, L. R. Walton, and A. H. Committee, "Wrought Tool Steels," in *Properties and Selection: Irons, Steels, and High-Performance Alloys*, vol. 1: ASM International, 1990, pp. 757-779.
[10] I. Gibson, D. W. Rosen, and B. Stucker, *Additive manufacturing technologies*. Springer, 2014.
[11] *MAGMASOFT®*. (1989-2018). Magma GmbH, Aachen, Germany. [Online]. Available: https://www.magmasoft.com/en/
[12] *LS-DYNA*. (1987-2020). Livermore Software Technology Corporation, Livermore, California. [Online]. Available: http://www.lstc.com/products/ls-dyna
[13] H. Yan, J. Hua, and R. Shivpuri, "Flow stress of AISI H13 die steel in hard machining," *Materials & design,* vol. 28, no. 1, pp. 272-277, 2007.
[14] "Varmint Al's Engineering page." http://www.varmintal.com/aengr.htm (accessed.
[15] G. Zhang, R. Batra, and J. Zheng, "Effect of frame size, frame type, and clamping pressure on the ballistic performance of soft body armor," *Composites Part B: Engineering,* vol. 39, no. 3, pp. 476-489, 2008.
[16] N. T. Roach and D. E. Lieberman, "Upper body contributions to power generation during rapid, overhand throwing in humans," *Journal of Experimental Biology,* vol. 217, no. 12, pp. 2139-2149, Jun 15 2014, doi: 10.1242/jeb.103275.
[17] G. R. Johnson and W. H. Cook, "A constitutive model and data for metals subjected to large strains, high strain rates and high temperatures," in *Proceedings of the 7th International Symposium on Ballistics*, 1983, vol. 21, no. 1: The Netherlands, pp. 541-547.